Equations (6), (19), and (22) now permit one to express $\mathbf{p}$ as

$$\mathbf{p} = \bar{a}_1\mathbf{c}_1 + \bar{a}_2\mathbf{c}_2 + [(J\bar{a}_3 + K\bar{r})/I]\mathbf{c}_3 \quad (23)$$

By construction, the unit vector $\mathbf{c}_3$ is parallel to a line that is fixed in both A and B. Thus, the angle θ between this line and the vector $\mathbf{p}$ is given by

$$\theta = \cos^{-1}(\mathbf{c}_3\cdot\mathbf{p}/|\mathbf{p}|) \quad (24)$$

or

$$\theta \underset{(23,24)}{=} \cos^{-1}\frac{J\bar{a}_3 + K\bar{r}}{[I^2(\bar{a}_1^2 + \bar{a}_2^2) + (J\bar{a}_3 + K\bar{r})^2]^{1/2}} \quad (25)$$

But $\mathbf{p}$ is parallel to $\mathbf{H}^G$, and $\mathbf{H}^G$ is fixed in N. Consequently, Eq. (25) gives the angle between the axis of revolution of E_B (or of E_G) and a line fixed in N.

Having determined the motion of C relative to N, we next consider the motions of A relative to C, and B relative to A. As regards the former, it is only necessary to recall that $\mathbf{s}$ denotes the angular velocity of A relative to C and to observe that Eqs. (5, 14, and 22) yield

$$\mathbf{s} = \{[(I - J)/J][(J\bar{a}_3 + K\bar{r})/I] - (K/J)r\}\mathbf{c}_3 \quad (26)$$

from which it is apparent that A spins relative to C with an angular speed that depends on the motion of B relative to A, that is, on r. Thus, the two motions under consideration are intimately related to each other, and an assumption regarding the interaction of A and B must be made before one can arrive at final expressions for $\mathbf{s}$ and $\mathbf{r}$. Three kinds of interaction will be considered: B constrained to remain fixed in A, so that G moves as a rigid body; B completely free to rotate relative to A (Leipholz's case); and B subjected to the action of a torque which retards rotation of B relative to A, the magnitude of the torque being taken proportional to the relative rotation rate r, as might be the case if forces are transmitted from A to B through a viscous medium.

The motion of B relative to A is governed by Eq. (18), which shows that B remains permanently fixed in A if $\mathbf{c}_3\cdot\mathbf{M} = 0$ and $r = 0$ at $t = 0$. In other words, strange as it may seem, no moment about the axis of rotation of B in A is required to prevent B from rotating relative to A. Expressions for $\mathbf{p}$, $\mathbf{s}$, and $\mathbf{r}$ suitable for the description of rigid body motions of G are [see Eqs. (23, 26, and 4)]

$$\mathbf{p}_R = \bar{a}_1\mathbf{c}_1 + \bar{a}_2\mathbf{c}_2 + \frac{J}{I}\bar{a}_3\mathbf{c}_3,\ \mathbf{s}_R = \frac{I - J}{I}\bar{a}_3\mathbf{c}_3,\ \mathbf{r}_R = 0 \quad (27)$$

If B is completely free to rotate relative to A, that is, if $\mathbf{c}_3\cdot\mathbf{M}$ is equal to zero, r, in accordance with Eq. (18), must remain constant, and thus equal to its initial value $\bar{r}$. The free rotor forms of $\mathbf{p}$, $\mathbf{s}$, and $\mathbf{r}$ are thus,

$$\mathbf{p}_F = \bar{a}_1\mathbf{c}_1 + \bar{a}_2\mathbf{c}_2 + [J\bar{a}_3 + K\bar{r}/I]\,\mathbf{c}_3$$

$$\mathbf{s}_F = \left(\frac{I - J}{I}\bar{a}_3 - \frac{K}{I}\bar{r}\right)\mathbf{c}_3,\ \mathbf{r}_F = \bar{r}\mathbf{c}_3 \quad (28)$$

Finally, when B's rotation relative to A is resisted by a torque whose magnitude is proportional to r, the right-hand member of Eq. (18) can be expressed as $-kr$, where k is a positive constant, and integration of Eq. (18) then yields $r = \bar{r}\exp(-kt)$ so that the expressions for $\mathbf{p}$, $\mathbf{s}$, and $\mathbf{r}$ associated with simple viscous damping are

$$\mathbf{p}_V = \bar{a}_1\mathbf{c}_1 + \bar{a}_2\mathbf{c}_2 + [(J\bar{a}_3 + K\bar{r})/I]\mathbf{c}_3 \quad (29)$$

$$\mathbf{s}_V = \left\{\frac{I - J}{I}\bar{a}_3 - \frac{K}{I}\bar{r}\left[1 - \frac{J}{I}\left(1 - e^{-kt}\right)\right]\right\}\mathbf{c}_3$$

$$\mathbf{r}_V = \bar{r}e^{-kt}\mathbf{c}_3 \quad (30)$$

Conclusion

The motion of G in N is completely characterized by the vectors $\mathbf{p}$, $\mathbf{s}$, and $\mathbf{r}$. General expressions for these are given in Eqs. (23, 26, and 4), respectively, where r denotes that solution of Eq. (18) which satisfies the condition $r = \bar{r}$ at $t = 0$. Special forms of the expressions for $\mathbf{p}$, $\mathbf{s}$, and $\mathbf{r}$ appear in Eqs. (27–30). Equation (23) shows that the angular velocity of precession is affected by rotation of B relative to A, but that only the initial value of the relative rotation rate, not its entire time history, plays a role. By way of contracts, the spin vector $\mathbf{s}$ and the relative rotation vector $\mathbf{r}$ depend intimately on the relative motion of A and B, as may be seen by reference to Eqs. (27, 28, and 30). Finally, Eq. (25) shows that the angle between the angular momentum of G with respect to G^* and the axis of revolution of the ellipsoid E_G remains constant regardless of the nature of the interaction of A and B. Thus, even in the presence of energy dissipation, there is no tendency for a gyrostat of the kind under consideration to "right" itself.

References

[1] Masaitis, C., "On the Motion of Two Linked Bodies," *Archive for Rational Mechanics and Analysis*, Vol. 8, 1961, pp. 23–25.

[2] Leipholz, H., "Ein Beitrag zu dem Problem des Kreisels mit drehzahlabhängiger Selbsterregung," *Ingenieur Archiv*, Vol. 32, No. 4, May 1963, pp. 255–285.

Stiffnesses of an Elastic Filler Constrained between a Rigid Sphere and a Rigid Ellipsoidal Shell

S. S. Chiu*
Sandia Laboratories, Livermore, Calif.

1. Introduction

THERE exists a structural dynamics problem, related to a flight vehicle, that deals with a spherical mass packaged inside an oblong shell. To predict the dynamic response of the vehicle, the stiffnesses of the filler must be determined. This problem is idealized to the case of a rigid sphere surrounded by an elastic filler which, in turn, is contained within a rotationally symmetric ellipsoidal shell (Fig. 1). The filler is assumed to have a low Poisson's ratio and to consist of nested ellipsoidal layers. Furthermore, the stresses in each layer are assumed to be distributed similarly and their magnitudes to vary inversely as the surface area of the layer. The effects of the spherical inclusion's motion, relative to the shell, on the stiffness of the elastic medium are calculated. A spherical outside shell is also considered as a limiting case of the ellipsoid. The results compare favorably with available analytical data.

2. Formal Statement of Problem

As explained later, the problem requires two sets of spherical coordinates (r,β,ξ) and (r,ϕ,θ) and the Cartesian coordinates (x,y,z). The relationships between the coordinates are

$$x = r\sin\beta\sin\xi = r\sin\phi\sin\theta \quad (1)$$

$$y = r\sin\beta\cos\xi = r\cos\phi \quad (2)$$

$$z = r\cos\beta = r\sin\phi\cos\theta \quad (3)$$

Received June 23, 1969; revision received February 24, 1970. This work was supported by the U. S. Atomic Energy Commission, Contract AT-(29-1)-789.

*Staff member, Analytical Mechanics Division.

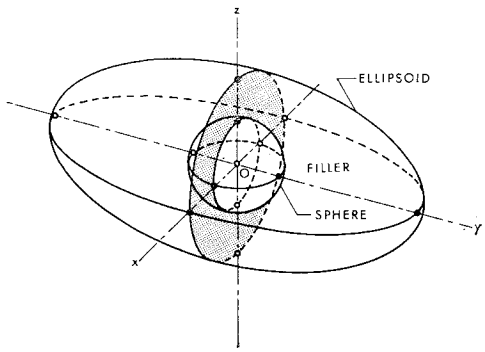

Fig. 1 General configuration.

$$r^2 = x^2 + y^2 + z^2 \tag{4}$$

A point on the ellipsoid (eccentricity designated e; major and minor semiaxes designated a and b, respectively) must obey

$$(x/b)^2 + (y/a)^2 + (z/b)^2 = 1 \tag{5}$$

$$r^2 = b^2/(1 - e^2\cos^2\phi),\ e^2 = 1 - (b/a)^2 \tag{6}$$

In the absence of body forces, the governing equations are

$$\nabla^2(u,v,w) + [1/(1-2\nu)](\partial/\partial x, \partial/\partial y, \partial/\partial z)\Delta = 0 \tag{7}$$

where u, v, and w are the displacements in the x, y, and z directions, respectively; ∇^2 is the Laplacian operator and Δ is the dilatation.

For determining the filler stiffness in the lateral mode, which relates the motion of the sphere along the z axis, the boundary conditions are given by

$$u = v = w = 0 \quad \text{at} \quad (x/b)^2 + (y/a)^2 + (z/b)^2 = 1 \tag{8}$$

$$u = v = 0,\ w = -w_0 \quad \text{at} \quad x^2 + y^2 + z^2 = c^2 \tag{9}$$

where w_0 is the vertical displacement of the sphere (radius designated c) under a vertical load (W), which may be taken as the weight of the sphere.

3. Method of Solution

Sternberg et al.[1] obtained an exact series solution for the limiting case of a sphere-in-sphere. However, an exact solution to the boundary value problem inherent in a sphere-in-ellipsoid does not seem possible. The usual numerical method for solving boundary value problems is the finite element approach, which has been successfully applied to axisymmetric problems.[2] In the closed-form method described herein, the approximate stiffnesses in both the axisymmetric and the nonaxisymmetric modes can be determined. (The latter case only is being presented.)

Average filler stresses

Using a generator line from the origin that meets the sphere at A and the ellipsoid at B, the thickness of the filler, h, is given by

$$h/b = AB/b = (r - c)/b = (1 - e^2\cos^2\phi)^{-1/2} - R \tag{10}$$

where $R = c/b$.

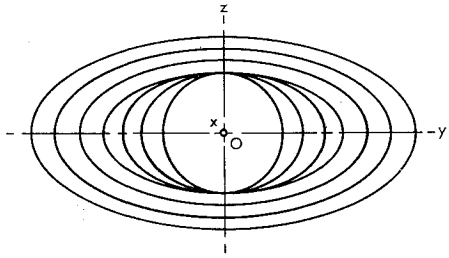

Fig. 2 Nested ellipsoids.

By means of a coordinate transformation, the radial and tangential displacements at the spherical boundary [Eq. (9)] become

$$(u_r)_{r=c} = -w_0\cos\beta,\ (u_\beta)_{r=c} = w_0\sin\beta \tag{11}$$

The average radial and shear strains acting in the meridional plane (ξ = const) are defined as the ratios of the corresponding displacements of the generator line over its length h. Thus

$$\epsilon_{\text{avg}} = (w_0/h)\cos\beta = \hat{\epsilon}_{\text{avg}}(b/h)(1 - R)\cos\beta \tag{12}$$

$$\gamma_{\text{avg}} = -(w_0/h)\sin\beta = -\epsilon_{\text{avg}}\tan\beta \tag{13}$$

where

$$\hat{\epsilon}_{\text{avg}} = (\epsilon_{\text{avg}})_{\beta=0} = (w_0/b)/(1 - R) \tag{14}$$

According to Hooke's law and the assumed negligible coupling caused by Poisson's effect, the radial stress and strain are proportional. Thus

$$\sigma_{\text{avg}} = \hat{\sigma}_{\text{avg}}(b/h)(1 - R)\cos\beta \tag{15}$$

No restrictions on Poisson's ratio are required when determining shear stresses. Thus, the average shear stress

$$\tau_{\text{avg}} = G\gamma_{\text{avg}} = -\hat{\sigma}_{\text{avg}}(b/h)(G/E)(1 - R)\sin\beta \tag{16}$$

Stress distribution in the filler

In determining the stress distribution in the filler, the following assumptions were made: 1) the filler is composed of nested layers, 2) the stress distribution in each layer is similar to the distribution of the average stresses, and 3) the stress magnitudes in each layer vary inversely with the surface area of the layer.

The layer configuration which is assumed consists of ellipsoidal layers. As shown in Fig. 2, the minor semiaxes of the inner layers are equal to the radius of the spherical cavity while the eccentricities of the inner layers increase from zero to that of the external shell. The eccentricity of the outer layers then remains constant.

Stresses at the filler cavity

The orthogonal coordinate system (r,β,ξ) was selected in determining the lateral stiffness because the shear stress, $\tau_{r\xi}$, which acts in the direction normal to the load can be disregarded. The remaining stress components at the cavity then are the radial stress σ_r and the shear stress $\tau_{r\beta}$. Based on these assumptions, the distribution of the stresses at the cavity is similar to that of the average values which is expressed by Eqs. (15) and (16). It follows that

$$\sigma_c = (\sigma_r)_{r=c} = \hat{\sigma}_c(b/h)(1 - R)\cos\beta \tag{17}$$

$$\tau_c = (\tau_{r\beta})_{r=c} = -\hat{\sigma}_c(b/h)(G/E)(1 - R)\sin\beta \tag{18}$$

where $\hat{\sigma}_c$ is the maximum radial stress at the cavity.

To sum up the tractions at the spherical cavity, vertical truncation is used with the spherical coordinates (r,ϕ,θ), since the resulting double integral can be reduced to a single one. Consequently, the use of two spherical coordinate systems, though seemingly unwieldy, has proven to be expedient.

The vertical component of the traction force acting on the spherical boundary can be found by multiplying the vertical stress resultant by the elemental area, $dA = c^2\sin\phi d\theta d\phi$, thus

$$dW = (\sigma_c\cos\beta - \tau_c\sin\beta)dA \tag{19}$$

Since the total traction force is in equilibrium with the applied load W,

$$W = \int_{\phi=0}^{\pi}\int_{\theta=-\pi}^{\pi} dW = 2\pi c^2(1 - R)\hat{\sigma}_c\left[2\frac{G}{E}I_1 + \left(1 - \frac{G}{E}\right)I_2\right] \tag{20}$$

where

$$I_n = \int_0^{\pi} \frac{\sin^{2n-1}\phi d\phi}{(1 - e^2\cos^2\phi)^{-1/2} - R} \quad (21)$$

The integrals can be evaluated in closed form as

$$I_1 = -\frac{1}{R} - \frac{1}{eR^2}\left[\text{arcsine} - \frac{\arctan\lambda + \arctan\mu}{(1 - R^2)^{1/2}}\right] \quad (22)$$

$$I_2 = -(1/e^2R)[1/R + \tfrac{2}{3}e^2 + (1/2R)(1 - e^2)^{1/2}] + (1/e^3R^2)(\tfrac{1}{2} - e^2 - R^2)\text{arcsine} + (1/e^2R^3)(\lambda + 1/\lambda)(\arctan\lambda + \arctan\mu) \quad (23)$$

where $\lambda = eR/(1 - R^2)^{1/2}$, $\mu = e/[(1 - e^2)(1 - R^2)]^{1/2}$. The numerical values for I_1 and I_2 show that they monotonically decrease with e but increase with R.

Lateral filler stiffness

Along the polar or z axis the assumed nested layers consist of ellipsoids having a constant eccentricity. In this case the surface area of an ellipsoid can be shown to be proportional to r^2, where r is the minor semiaxis of an ellipsoid in the nested layers. According to the assumptions, the maximum radial strain in a layer can be related to the corresponding value at the cavity by

$$\hat{\epsilon}_r = (c/r)^2\hat{\epsilon}_c \quad c \leqq r \leqq b \quad (24)$$

Since the maximum radial strains occur along the z axis ($\beta = 0$) where the shear strains $\gamma_{r\beta}$ vanish, the total displacement along this axis becomes

$$w_0 = \int_c^b \hat{\epsilon}_r dr = c^2\hat{\epsilon}_c \int_c^b \frac{1}{r^2}\, dr = c(1 - R)\hat{\epsilon}_c \quad (25)$$

The lateral stiffness then becomes

$$K = W/w_0 = 2\pi cE[2(G/E)I_1 + (1 - G/E)I_2] \quad (26)$$

Of interest is the spherical shell representing the limiting condition of the ellipsoid. When $e = 0$, Eq. (26) becomes

$$K_{\text{sphere}} = [4\pi cE/3(1 - R)](1 + 2G/E) = [8\pi cG/3(1 - R)](2 + \nu) \quad (27)$$

where ν is Poisson's ratio.

4. Results

The stiffness of the filler [Eq. (26)] is a function of: 1) the geometric parameters of the spherical cavity and the external ellipsoidal shell and 2) the material properties. To investigate the functional dependencies, it is desirable to express the stiffness in nondimensional form, K, which is defined by

$$K = \frac{K_{\text{ellipsoid}}}{K_{\text{sphere}}} = \frac{3}{2}\frac{1 - R}{1 + 2G/E}\left[2\frac{G}{E}I_1 + \left(1 - \frac{G}{E}\right)I_2\right] \quad (28)$$

Thus, $K = K(e,R;G/E)$ since I_1 and I_1 [Eq. (21)] are functions of e and R.

If R and G/E are kept constant, a variation of e is equivalent to a variation in the axial dimension of the ellipsoidal shell. Figure 3 shows that K decreases as e, or the volume of the filler, increases. Analogously, the filler can be considered as a spring whose effective length increases as the volume of the filler increases, causing the spring to become softer.

Keeping e constant, a variation in b results in a change in the size of the ellipsoidal shell. Without losing generality, if c is kept constant, the shell size increases directly with b and inversely with R. The relationship between K and R that results when the other parameters are held constant is illustrated in Fig. 4.

For most materials the Poisson's ratios are limited in the range $0 \leqq \nu \leqq \frac{1}{2}$ which implies $\frac{1}{2} \geqq G/E \geqq \frac{1}{3}$. Since $\nu = \frac{1}{2}$ signifies an incompressible material, it is a true upper bound. However, the use of $\nu > \frac{1}{2}$ (or $G/E < \frac{1}{3}$), in Figs. 3 and 4 does not imply unrealistic materials, but rather a redefinition of the problem; it can be shown that the solution for the case of vanishing shear stress can be obtained by setting $G/E = 0$, which applies to the case of a filler that is not bonded to the housing.

Table 1 Comparison of the exact and approximate solutions in the axial mode of the spherical case

	Exact $f(\nu,R)$					Approximate
ν	$R = 0$	0.25	0.50	0.75	0.90	$(2 + \nu)$
0	1.80	1.84	1.89	1.92	1.92	2.00
0.25	1.93	2.03	2.13	2.20	2.22	2.25
0.33	2.00	2.14	2.30	2.40	2.43	2.33

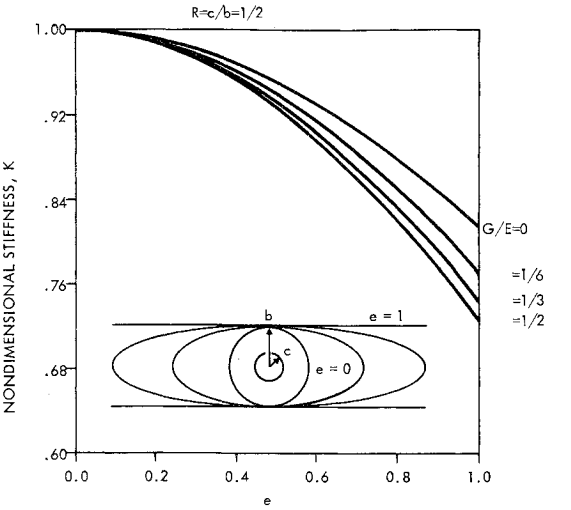

Fig. 3 Effects of variation in axial dimension of the external shell ($R = c/b = \frac{1}{2}$).

5. Evaluation

For the limiting case of the sphere-in-sphere, exact solutions are available which can be used to check the validity of the approximate closed-form method. For the stiffness in the torsional mode an exact solution, using the semi-inverse method, can be obtained which agrees identically with the present solution. This is not so surprising since the assumptions are satisfied identically.

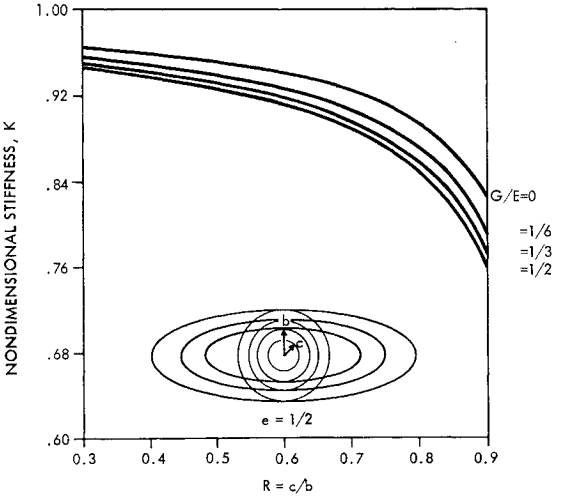

Fig. 4 Effects of variation in size of shells with constant eccentricity ($e = \frac{1}{2}$).

For the stiffnesses in the axial mode, the exact solution for the sphere-in-sphere[1] can be shown to be

$$K = \frac{W}{w_0} = \frac{8\pi cG}{3(1-R)} f(\nu,R) \tag{29}$$

where

$$f(\nu,R) = \frac{3(1-\nu)(5-6\nu)}{9-20\nu+12\nu^2-2(1-R^3)^2/3(1-R)(1-R^5)}$$

The resulting stiffness can be compared with the corresponding approximate solution [Eq. (27)]. These results differ in the last term only. Consequently, these factors alone are used in the comparative study (results listed in Table 1). The exact solution portion, $f(\nu,R)$, is a function of R while its approximate counterpart is not. The approximate solution agrees within 6% for $R \geqq \frac{1}{2}$ which represents the range of practical interest ($R = 0$ implies an infinitely large filler). The agreement is closer using smaller values of Poisson's ratio which happen to comply well with the assumption made in the approximate closed-form solution.

References

[1] Sternberg, E., Eubanks, R. A., and Sadowsky, M. A., "On the Axisymmetric Problem of Elasticity Theory for a Region Bounded by Two Concentric Spheres," *First U.S. National Congress of Applied Mechanics*, 1952, pp. 209–215.

[2] Wilson, E. L., "Structural Analysis of Axisymmetric Solids," *AIAA Journal*, Vol. 3, No. 12, Dec. 1965, pp. 2269–2274.

An Evaluation of a Transfer Coefficient Approach for Unequal-Diffusion Coefficients

RONALD D. GROSE* AND EUGENE P. BARTLETT†
Aerotherm Corporation, Mountain View, Calif.

1. Introduction

IN a recent AIAA paper,[1] Kendall, Rindal, and Bartlett postulated a procedure that provides a significant simplification for solving ablative-material-coupled, unequal-diffusion, multicomponent boundary-layer problems. The procedure employs correlation equations that directly relate boundary-layer edge conditions to the ablative surface condition through transfer coefficients and driving potentials. The form of the driving potentials was suggested by terms in the differential equations that were derived using a special treatment of diffusion coefficients (termed a bifurcation approximation).

It is the purpose of this Note to describe the extent to which successful validation of this approach has been achieved and to present values for the arbitrary parameters involved. This was accomplished using the results of "exact" solutions of the differential equations obtained with the numerical solution procedure described in Ref. 2. Solutions were obtained for two representative materials, graphite and nylon phenolic, and five flight conditions at the stagnation point of a hemispherical re-entry body having a radius of 1 in. In these calculations, the boundary layer is fully coupled with the ablative-material response; the wall boundary condition satisfying the elemental mass balances, a steady-state energy balance, and surface equilibrium.

2. Summary of the Unequal-Diffusion Film Analogy

The extension of the simple film transport concept to describe unequal-diffusion effects was based on a modeling of the governing differential equations describing the process. Such modeling was accomplished in Ref. 1 to which the reader seeking a description of the mathematical development is directed. The pertinent concepts of the method are:

1) In the bifurcation approximation to the boundary-layer elemental species equation, the diffusive term contains the gradient of a newly-defined species elemental fraction, $\tilde{Z}_k$, (the elemental mass fraction still appearing in the convection terms). The analogy between this equation and its equal-diffusion counterpart, in conjunction with a film-transport correlation equation for equal diffusion, leads to the following correlation equation for unequal diffusion:

$$\tilde{j}_{kw} = \rho_e U_e C_{M_k} (\tilde{Z}_{k_w}{}^* - \tilde{Z}_{k_e}{}^*) \tag{1}$$

The driving potential $\tilde{Z}_k{}^*$ is a geometrically weighted average between the driving potentials applicable to the convective and diffusional terms that appear in the differential equation. An arbitrary weighting factor γ suggested in Ref. 1 to have a value of $\frac{2}{3}$, appears in the definition for $\tilde{Z}_k{}^*$. A primary purpose for introducing the $\tilde{Z}_k{}^*$ potential is to attempt to reduce the C_{M_k} to a single C_M through appropriate choice of γ. The success of this approach is one of the principal findings of this Note.

2) The wall energy flux is conveniently divided into terms representing two processes: diffusion of chemical energy at some base temperature and convection of sensible enthalpy measured above this base temperature.[3] In Ref. 1, a film-coefficient correlation equation is suggested having terms corresponding to these two processes. The first is represented by a mean (or over-all effective) mass-transfer coefficient and a weighted species-enthalpy driving potential, the second by a heat-transfer coefficient and a sensible enthalpy driving potential. The form of the equation presented in Ref. 1 is based on the arbitrary choice of the wall temperature as the base temperature. More generally, the energy equation with arbitrary base temperature is

$$q_w = \rho_e U_e C_M \sum_i (Z_{i_e}{}^* - Z_{i_w}{}^*) h_{ib} + \rho_e U_e C_H \times \left[(H_{s_r} - h_{sb})_e - \sum_i K_{iw} (h_{iw} - h_{ib}) \right] \tag{2}$$

where K_i and h_i are the mass fraction and enthalpy of species i, h_s and H_{s_r} are sensible and recovery enthalpies, and the b, w, and e subscripts denote base temperature, wall, and boundary-layer edge composition, respectively. The influence of the base temperature also is established in this Note.

3. Mass-Transfer Coefficient Results

Two ablative materials, graphite and nylon phenolic, were evaluated over a range of representative earth-ballistic-reentry conditions using computer codes in which both the exact and foregoing film-analogy equations were programed.[2,4] A summary of the elemental mass-transfer coefficient results are presented in Fig. 1. These results were obtained from Eq. (1) with both the elemental flux at the wall $\tilde{j}_{kw}$ and the driving potentials $\tilde{Z}_k{}^*$ obtained from the "exact" steady-state solutions.

For the three-element graphite solutions, precise crossovers occur since there are only N-1 = 2 independent elemental conservation equations.[5] The crossover points are seen to occur at values of γ varying from 0.3–0.7. In the case of the four-element nylon-phenolic solutions, unique crossovers are not generally obtained; however, the curves do demonstrate

Received June 12, 1969. This work was supported by U.S. Atomic Energy Commission under contract to Sandia Laboratories and Sandia contract to Aerotherm Corporation Contract No. 48-7407.

* Staff Engineer, Analytical Services Division. Member AIAA.

† Manager, Aerochemistry Department, Analytical Services Division. Member AIAA.